

# Ten dimensional Wavepacket Simulations of Methane Scattering.

R. Milot and A.P.J. Jansen

*Schuit Institute of Catalysis, T/TAK, Eindhoven University of Technology*

*P.O. Box 513, NL-5600 MB Eindhoven, The Netherlands*

(November 5, 2018)

We present results of wavepacket simulations of scattering of an oriented methane molecule from a flat surface including all nine internal vibrations. At a translational energy up to 96 kJ/mol we find that the scattering is almost completely elastic. Vibrational excitations when the molecule hits the surface and the corresponding deformation depend on generic features of the potential energy surface. In particular, our simulation indicate that for methane to dissociate the interaction of the molecule with the surface should lead to an elongated equilibrium C–H bond length close to the surface.

## I. INTRODUCTION

The dissociation of methane on transition metals is an important reaction in catalysis. It is the rate limiting step in steam reforming to produce syngas.<sup>1</sup> It is also prototypical for C–H activation in other processes. A large number of molecular beam experiments in which the dissociation energy was measured as a function of translational energy<sup>2–18</sup> as well as various bulb gas experiments<sup>19–24</sup> have already been done on this system. These experiments have contributed much to our understanding of the mechanism of the dissociation. However, our knowledge is still small compared to what we know about a well-studied reaction as H<sub>2</sub> dissociation.

Some years ago we performed a multi-configurational time-dependent Hartree (MCTDH) study of CH<sub>4</sub> dissociation on Ni(111)<sup>25</sup> with a potential energy surface (PES) based on our earlier density functional theory (DFT) calculations.<sup>26–30</sup> We included the distance of the methane molecule to the surface, a C–H distance, and the orientation of methane as coordinates. Other wavepacket simulations focused on (some of) these coordinates in combination with lattice motion on several metals.<sup>31–34</sup> Other theoretical studies on this system used DFT calculations<sup>35–37</sup> too and classical stochastic trajectory simulations.<sup>38,39</sup>

None of the wavepacket simulations published so far have looked at the role of the internal vibrations of methane. It was observed experimentally that vibrationally hot CH<sub>4</sub> dissociates more readily than cold CH<sub>4</sub>, with the energy in the internal vibrations being about as effective as the translational energy in inducing dissociation.<sup>2,3,5,8,10</sup> However, a more detailed assessment of the importance of the internal vibrations could not be made, because of the large number of internal vibrations. A recent DFT calculation also showed that the transition state for CH<sub>4</sub> dissociation on Ni(111) involves considerable internal excitation of the molecule.<sup>35</sup> In this paper we report on wavepacket simulations that we have done to determine which and to what extent internal vibrations are important for the dissociation. We are not able yet to simulate the dissociation including all internal vibrations. Instead we have simulated the scattering of methane, for which all internal vibrations can be included. By looking at vibrational excitations and the deformation of the molecule when it hits the surface we can derive information that is relevant for the dissociation. We have used PESs that have been developed with Ni(111) in mind, but our results should hold for other surfaces as well.

We have again used the MCTDH method for the wavepacket simulations, because it can deal with a large number of degrees of freedom and with large grids.<sup>40,41</sup> This method has been applied successfully to gas phase reactions and reactions at surfaces.<sup>42–53</sup>

The rest of this paper is organized as follows. We start with a brief description of the MCTDH method. Then the various PESs that we have used are derived. (A harmonic intramolecular PES is adapted to include anharmonicities in the C–H distance, the decrease of the C–H bond energy due to interactions with the surface, and the increase of the C–H bond length also due to interactions with the surface.) The results of the simulations are presented and discussed next. We focus on excitation probabilities and deformation of the molecule when it hits the surface. The implications for the dissociation are discussed separately. We end with a summary and some general conclusions.

## II. COMPUTATIONAL DETAILS

## A. The MCTDH Method

We give here a short overview of the MCTDH approximation for completeness. More details can be found in Refs. 40 and 41. The exact wave-function of a  $D$ -dimensional system, is approximated by an expression of the form

$$\Psi_{\text{MCTDH}}(q_1, \dots, q_D; t) = \sum_{n_1 \dots n_D} c_{n_1 \dots n_D}(t) \psi_{n_1}^{(1)}(q_1; t) \dots \psi_{n_D}^{(D)}(q_D; t). \quad (1)$$

From this expression, it is possible to obtain the equations of motion for the one-dimensional functions  $\psi_{n_i}^{(i)}(q_i; t)$  and for the correlation coefficients  $c_{n_1 \dots n_D}(t)$ . Without loss of generality we can choose the  $\psi_{n_i}^{(i)}$ 's to be natural single-particle states.<sup>41</sup> They insure that we obtain the best approximation to the exact  $\Psi(q_1, \dots, q_D; t)$  for a fixed number of configurations; i.e., they minimize the expression  $\langle \Delta | \Delta \rangle$  where

$$\Delta = \Psi - \Psi_{\text{MCTDH}}, \quad (2)$$

and where  $\Psi$  is the exact wave-function. The natural single-particle functions are eigenstates of the reduced density operators.

$$\rho_j(q_j, q'_j) = \int dq_1 \dots dq_{j-1} dq_{j+1} \dots dq_D \Psi(q_1 \dots q_{j-1} q_j q_{j+1} \dots q_D) \Psi^*(q_1 \dots q_{j-1} q'_j q_{j+1} \dots q_D). \quad (3)$$

The equations of motions for the natural single-particle states can be obtained by differentiation of the eigenvalue equation:

$$\int dq'_j \rho_j(q_j, q'_j) \psi_n^{(i)}(q'_j) = \nu_n^{(i)} \psi_n^{(i)}(q_j). \quad (4)$$

This gives us

$$i\hbar \frac{\partial}{\partial t} \psi_{n_j}^{(j)} = h_j \psi_{n_j}^{(j)} + \sum_{m_j} B_{n_j m_j}^{(j)} \psi_{m_j}^{(j)} + \frac{\langle \tilde{\psi}_{n_j}^{(j)} | V | \Psi \rangle}{\langle \tilde{\psi}_{n_j}^{(j)} | \tilde{\psi}_{n_j}^{(j)} \rangle} - \sum_{m_j} \frac{\langle \psi_{m_j}^{(j)} \tilde{\psi}_{n_j}^{(j)} | V | \Psi \rangle}{\langle \tilde{\psi}_{n_j}^{(j)} | \tilde{\psi}_{n_j}^{(j)} \rangle} \psi_{m_j}^{(j)}, \quad (5)$$

where

$$B_{n_j m_j}^{(j)} = \frac{\langle \psi_{m_j}^{(j)} \tilde{\psi}_{n_j}^{(j)} | V | \Psi \rangle - \langle \Psi | V | \psi_{n_j}^{(j)} \tilde{\psi}_{m_j}^{(j)} \rangle}{\langle \tilde{\psi}_{n_j}^{(j)} | \tilde{\psi}_{n_j}^{(j)} \rangle - \langle \tilde{\psi}_{m_j}^{(j)} | \tilde{\psi}_{m_j}^{(j)} \rangle}, \quad (6)$$

and

$$\tilde{\psi}_{n_j}^{(j)} = \sum_{n_1 \dots n_{j-1}} \sum_{n_{j+1} \dots n_D} c_{n_1 \dots n_D} \psi_{n_1}^{(1)} \dots \psi_{n_{j-1}}^{(j-1)} \psi_{n_{j+1}}^{(j+1)} \dots \psi_{n_D}^{(D)}, \quad (7)$$

with the Hamiltonian  $H$  given by

$$H = \sum_{j=1}^D h_j + V. \quad (8)$$

The equations of motion for the coefficients

$$c_{n_1 \dots n_D} = \langle \psi_{n_1}^{(1)} \dots \psi_{n_D}^{(D)} | \Psi \rangle \quad (9)$$

are again obtained by differentiation.

$$i\hbar \frac{d}{dt} c_{n_1 \dots n_D} = \langle \psi_{n_1}^{(1)} \dots \psi_{n_D}^{(D)} | V | \Psi \rangle - \sum_{j=1}^D c_{n_1 \dots n_{j-1} m_j n_{j+1} \dots n_D} B_{m_j n_j}^{(j)}. \quad (10)$$

Equations (5) and (10) are a particular form of the more general equations obtained from a time-dependent variational principle.<sup>40</sup> They conserve the norm of the wave-function and the mean energy of a time-independent Hamiltonian.

The resulting system of first-order differential equations, has to be solved with a general-purpose integrator. We used the variable-order variable-step Adams method, as implemented in the NAG library.<sup>54</sup> This method gave good convergence for all described simulations. For the hardest simulation the method needed 195027 calculations of the time derivatives for 35000 atomic units simulation time, which took around two days CPU-time on an 166 MHz. SUN Ultra SPARC. The singularities in Eqs. (5), (6), and (10) have been treated numerically by the regularization procedure described in Ref. 41.

The natural single-particle states have some small advantages over other possible choices of single-particle states. The most important one is that one can directly see from  $\langle \tilde{\psi}_n^{(i)} | \tilde{\psi}_n^{(i)} \rangle$  how well  $\Psi_{\text{MCTDH}}$  approximates the exact wavefunction. How much a natural single-particle functions contributes to the wavefunction is given by the eigenvalue  $\nu_n^{(i)}$  of the reduced density matrix. In an approximate MCTDH simulation  $\langle \tilde{\psi}_n^{(i)} | \tilde{\psi}_n^{(i)} \rangle$  is an approximation for this exact eigenvalue. The natural single-particle functions are also convenient for interpreting the results of a simulations.

## B. The Potential Energy Surfaces

The PESs we used can all be written as

$$V_{\text{total}} = V_{\text{intra}} + V_{\text{surf}}, \quad (11)$$

where  $V_{\text{intra}}$  is the intramolecular PES and  $V_{\text{surf}}$  is the interaction with the surface. For the  $V_{\text{intra}}$  we looked at four different types of PESs.

### 1. A harmonic potential

The first one is completely harmonic. We have used normal mode coordinates for the internal vibrations, because these are coupled only very weakly. In the harmonic approximation this coupling is even absent so that we can write  $V_{\text{intra}}$  as

$$V_{\text{intra}} = V_{\text{harm}} = \frac{1}{2} \sum_{i=2}^{10} k_i X_i^2, \quad (12)$$

the summation is over the internal vibrations,  $X_i$ 's are mass-weighted displacement coordinates and  $k_i$  are mass-weighted force constants. (see Table I for definitions and values); ( $X_1$  is the mass-weighted overall translation along the surface normal).<sup>55</sup> The force constants have been obtained by fitting them on the experimental vibrational frequencies of  $\text{CH}_4$  and  $\text{CD}_4$ .<sup>56,57</sup>

We have assumed that the interaction with the surface is only through the hydrogen atoms that point towards the surface. We take the  $z$ -axis as the surface normal. In this case the surface PES is given by

$$V_{\text{surf}} = \frac{A}{N_H} \sum_{i=1}^{N_H} e^{-\alpha z_i}, \quad (13)$$

where  $N_H$  is the number of hydrogens that points towards the surface,  $\alpha=1.0726$  atomic units and  $A=6.4127$  Hartree. These parameters are chosen to give the same repulsion as the PES that has been used in an MCTDH wavepacket simulation of  $\text{CH}_4$  dissociation.<sup>25</sup>

If we write  $V_{\text{surf}}$  in terms of normal mode coordinates, then we obtain for one hydrogen pointing towards the surface

$$V_{\text{surf}} = A e^{-\alpha_1 X_1} e^{-\alpha_2 X_2} e^{-\alpha_3 X_3} e^{-\alpha_4 X_4}, \quad (14)$$

where  $A$  as above, and  $\alpha$ 's as given in Table II.  $X_2$ ,  $X_3$  and  $X_4$  correspond all to  $a_1$  modes of the  $\text{C}_{3v}$  symmetry. There is no coupling between the modes  $X_5$  to  $X_{10}$  in the  $V_{\text{surf}}$  part of the PES, which are all  $e$  modes of the  $\text{C}_{3v}$  symmetry. Fig. 1(a) shows a contour plot of the cross-section of the total harmonic PES with one hydrogen pointing towards the surface in the translational mode  $X_1$  and the  $\nu_3$  asymmetrical stretch mode  $X_4$ .

For two hydrogens we obtain

$$\begin{aligned} V_{\text{surf}} = & A e^{-\alpha_1 X_1} e^{-\alpha_2 X_2} e^{-\alpha_3 X_3} e^{-\alpha_4 X_4} e^{-\alpha_5 X_5} \\ & \times \frac{1}{2} \left[ e^{\beta_3 X_7} e^{-\beta_3 X_8} e^{-\beta_5 X_9} e^{\beta_5 X_{10}} \right. \\ & \left. + e^{-\beta_3 X_7} e^{\beta_3 X_8} e^{\beta_5 X_9} e^{-\beta_5 X_{10}} \right], \end{aligned} \quad (15)$$

with  $A$  again as above,  $\alpha$ 's and  $\beta$ 's as given in Table II.  $X_2$ ,  $X_3$ ,  $X_4$  and  $X_5$  correspond all to  $a_1$  modes of  $C_{2v}$ .  $X_7$ ,  $X_8$ ,  $X_9$  and  $X_{10}$  correspond to  $b_1$  and  $b_2$  modes of  $C_{2v}$ .  $X_6$  corresponds to the  $a_2$  mode of  $C_{2v}$  and has no coupling with the other modes in  $V_{\text{surf}}$ .

For three hydrogens we obtain

$$V_{\text{surf}} = A e^{-\alpha_1 X_1} e^{-\alpha_2 X_2} e^{-\alpha_3 X_3} e^{-\alpha_4 X_4} \times \frac{1}{3} \left[ e^{\beta_1 X_5} e^{\beta_2 X_6} e^{-\beta_3 X_7} e^{-\beta_4 X_8} e^{\beta_5 X_9} e^{\beta_6 X_{10}} + e^{\beta_1 X_5} e^{-\beta_2 X_6} e^{-\beta_3 X_7} e^{\beta_4 X_8} e^{\beta_5 X_9} e^{-\beta_6 X_{10}} + e^{-2\beta_1 X_5} e^{2\beta_3 X_7} e^{-2\beta_5 X_9} \right], \quad (16)$$

$X_2$ ,  $X_3$  and  $X_4$  corresponds to  $a_1$  modes in the  $C_{3v}$  symmetry. Because these last six coordinates correspond to degenerate  $e$  modes of the  $C_{3v}$  symmetry, the  $\beta$  parameters are not unique.

## 2. An anharmonic intramolecular potential

Even though we do not try to describe the dissociation of methane in this paper, we do want to determine which internal vibration might be important for this dissociation. The PES should at least allow the molecule to partially distort as when dissociating. The harmonic PES does not do this. A number of changes have therefor been made. The first is that we have describe the C–H bond by a Morse PES.

$$V_{\text{Morse}} = D_e \sum_{i=1}^4 \left[ 1 - e^{-\gamma \Delta r_i} \right]^2, \quad (17)$$

where  $D_e = 0.1828$  Hartree (the dissociation energy of methane in the gas-phase) and  $\Delta r_i$  the change in bond length from the equilibrium distance.  $\gamma$  was calculated by equating the second derivatives along one bond of the harmonic and the Morse PES. If we transform Eq. (17) back into normal mode coordinates, we obtain

$$V_{\text{Morse}} = D_e \sum_{i=1}^4 \left[ 1 - e^{\gamma_{i2} X_2} e^{\gamma_{i3} X_3} e^{\gamma_{i4} X_4} e^{\gamma_{i7} X_7} e^{\gamma_{i8} X_8} e^{\gamma_{i9} X_9} e^{\gamma_{i,10} X_{10}} \right]^2, \quad (18)$$

with  $D_e$  as above.  $\gamma$ 's are given in Tables III and IV. Note that, although we have only changed the PES of the bond lengths, the  $\nu_4$  umbrella modes are also affected. This is because these modes are not only bending, but also contain some changes of bond length.

The new intramolecular PES now becomes

$$V_{\text{intra}} = V_{\text{harm}} + V_{\text{Morse}} - V_{\text{corr}}, \quad (19)$$

where  $V_{\text{harm}}$  is as given in Eq. (12) and  $V_{\text{corr}}$  is the quadratic part of  $V_{\text{Morse}}$ , which is already in  $V_{\text{harm}}$ . Fig. 1(b) shows a contour plot of the cross-section of this total anharmonic PES with one hydrogen pointing towards the surface in the translational mode  $X_1$  and the  $\nu_3$  asymmetrical stretch mode  $X_4$ . (We would like to point out that there are, of course, various anharmonic PESs for methane in the literature. There are two reasons why we haven't use them. First, these PESs are not in appropriate form to use then with the MCTDH method.<sup>40,41</sup> Second, these PESs are generally quite complicated. We prefer to keep it as simple as possible, because at this moment we're only interested in qualitative effects.)

## 3. Intramolecular potential with weakening C–H bonds

When the methane molecule approach the surface the overlap of substrate orbitals and anti-bonding orbitals of the molecule weakens the C–H bonds. We want to include this effect for the C–H bonds of the hydrogens pointing towards the surface. We have redefined the  $V_{\text{Morse}}$  given in Eq. (18) and also replace it in Eq. (19). A sigmoidal function is used to switch from the gas phase C–H bond to a bond close to the surface. We have used the following, somewhat arbitrary, approximations. (i) The point of inflection should be at a reasonable distance from the surface. It is set to the turnaround point for a rigid methane molecule with translation energy 93.2 kJ/mol plus twice the fall-off distance

of the interaction with the surface. (ii) The depth of the PES of the C–H bond is 480 kJ/mol in the gas phase, but only 93.2 kJ/mol near the surface. The value 93.2 kJ/mol corresponds to the height of the activation barrier used in our dissociation.<sup>25</sup> (iii) The exponential factor is the same as for the interaction with the surface.

If we transform to normal-mode coordinates for the particular orientations, we then obtain

$$V_{\text{weak}} = D_e \sum_{i=1}^4 W_i \left[ 1 - e^{\gamma_{i2} X_2} e^{\gamma_{i3} X_3} e^{\gamma_{i4} X_4} e^{\gamma_{i7} X_7} e^{\gamma_{i8} X_8} e^{\gamma_{i9} X_9} e^{\gamma_{i,10} X_{10}} \right]^2, \quad (20)$$

where  $W_i = 1$  for non-interacting bonds and

$$W_i = \frac{1 + \Omega e^{-\alpha_1 X_1 + \omega}}{1 + e^{-\alpha_1 X_1 + \omega}} \quad (21)$$

for the interacting bonds pointing towards the surface.  $\alpha_1$  is as given in Table II,  $\gamma$ 's are given in Tables III and IV,  $\Omega = 1.942 \cdot 10^{-1}$  and  $\omega = 7.197$ . Fig. 1(c) shows a contour plot of the cross-section of this total anharmonic PES with weakening C–H bond for the orientation with one hydrogen pointing towards the surface in the translational mode  $X_1$  and the  $\nu_3$  asymmetrical stretch mode  $X_4$ .

#### 4. Intramolecular potential with elongation of the C–H bond

A weakened bond generally has not only a reduced bond strength, but also an increased bond length. We include the effect of the elongation of the C–H bond length of the hydrogens that point towards the surface due to interactions with the surface. We have redefined the  $V_{\text{Morse}}$  given in Eq. (18) and also replace it in Eq. (19) for this type of PES. We have used the following approximations: (i) The transition state, as determined by Refs. 27,28, has a C–H bond that is 0.54 Å longer than normal. This elongation should occur at the turn around point for a rigid methane molecule with a translation energy of 93.2 kJ/mol. (ii) The exponential factor is again the same as for the interaction with the surface.

If we transform to normal-mode coordinates for the particular orientations, then we obtain

$$V_{\text{shift}} = D_e \sum_{i=1}^4 \left[ 1 - e^{\gamma_{i2} X_2} e^{\gamma_{i3} X_3} e^{\gamma_{i4} X_4} e^{\gamma_{i7} X_7} e^{\gamma_{i8} X_8} e^{\gamma_{i9} X_9} e^{\gamma_{i,10} X_{10}} \exp[S_i e^{-\alpha_1 X_1}] \right]^2, \quad (22)$$

where  $\alpha_1$  is as given in Table II,  $\gamma$ 's are given in Tables III and IV. For orientation with one hydrogen towards the surface we obtain;  $S_1 = 2.942 \cdot 10^2$  and  $S_2 = S_3 = S_4 = 0$ , with two hydrogens;  $S_1 = S_2 = 0$  and  $S_3 = S_4 = 1.698 \cdot 10^2$ , and with three hydrogens;  $S_1 = 0$  and  $S_2 = S_3 = S_4 = 2.942 \cdot 10^2$ . Fig. 1(d) shows a contour plot of the cross-section of this total anharmonic PES with elongation of the C–H bond for the orientation with one hydrogen pointing towards the surface in the translational mode  $X_1$  and the  $\nu_3$  asymmetrical stretch mode  $X_4$ , and Fig. 2 shows a contour plot of a cross-section in the translational  $X_1$  and the  $\nu_1$  asymmetrical stretch mode  $X_2$  in the three different orientations.

Finally we like to note that the monotonic behaviour of all PES types in the translational mode does not contradict with the fact that the dissociative adsorption of methane is activated. The activation barrier for dissociative adsorption in the translational mode is situated in a region with very high excitations of the stretch modes, which we do not reach in these simulations.

### C. Initial States

All initial states in the simulations start with the vibrational ground state. The initial translational part  $\psi^{(\text{tr})}$  is represented by a Gaussian wave-packet,

$$\psi^{(\text{tr})}(X_1) = (2\pi\sigma^2)^{-1/4} \exp \left[ -\frac{(X_1 - X_0)^2}{4\sigma^2} + iP_1 X_1 \right], \quad (23)$$

where  $\sigma$  is the width of the wave-packet (we used  $\sigma = 320.248$  atomic units),  $X_0$  is the initial position (we used  $X_0 = 11\sigma$ , which is far enough from the surface to observe no repulsion) and  $P_1$  is the initial momentum. We performed simulations in the energy range of 32 to 96 kJ/mol. We here present only the results of 96 kJ/mol (equivalent to  $P_1 = 0.2704$  atomic units), because they showed the most obvious excitation probabilities for  $V_{\text{Morse}}$ .

We used seven natural single-particle states, 512 grid points and a grid-length of  $15\sigma$  for the translational coordinate. With this grid-width we can perform simulation with a translational energy up to 144 kJ/mol.

Gauss-Hermite discrete-variable representations (DVR)<sup>58</sup> were used to represent the wavepackets of the vibrational modes. We used for all simulations 5 DVR points for the  $\nu_2$  bending modes and 8 DVR points for the  $\nu_4$  umbrella,  $\nu_3$  asymmetrical stretch, and  $\nu_1$  symmetrical stretch mode for an numerical exact integration, except for the simulations with  $V_{\text{shift}}$ , where we used 16 DVR points for the  $\nu_1$  symmetrical stretch mode, because of the change in the equilibrium position.

We did the simulation with one hydrogen pointing towards the surface in eight dimensions, because the  $\nu_2$  bending modes  $X_5$  and  $X_6$  do not couple with the other modes. We needed four natural single-particle states for modes  $X_2$ ,  $X_3$  and  $X_4$ , and just one for the others. So the number of configurations was  $7^1 \cdot 4^3 \cdot 1^4 = 448$ . The simulation with two hydrogens pointing towards the surface was performed in nine dimensions. One of the  $\nu_2$  bending mode ( $X_6$ ) does not couple with the other modes, but for the other mode  $X_5$  we needed four natural single-particle states. The number of configurations was  $7^1 \cdot 4^4 \cdot 1^4 = 1792$ , because we needed the same number of natural single-particle states as mentioned above for the other modes. We needed ten dimensions to perform the simulation with three hydrogens pointing towards the surface. We used here one natural single-particle state for the modes  $X_5$  to  $X_{10}$  and four natural single-particle states for  $X_2$  to  $X_4$ , which gave us  $7^1 \cdot 4^3 \cdot 1^6 = 448$  configurations.

### III. RESULTS AND DISCUSSION

We found that the scattering is predominantly elastic. The elastic scattering probability is larger than 0.99 for all orientations and PESs at a translational energy of 96 kJ/mol, except for the PES with  $V_{\text{shift}}$  and three hydrogens pointing towards the surface for which it is 0.956. This agrees with the observation that the translation-vibration coupling is generally small.<sup>59</sup>

If we would have wanted to determine the role of the internal vibrations from the scattering probabilities, we would have to do quite accurate simulations. We have opted instead to look at the molecule when it hits the surface, which enables us to obtain good results with much less costly simulations.

#### A. Excitation Probabilities

The surface PES has  $C_{3v}$  (with one or three hydrogens towards the surface) or  $C_{2v}$  symmetry (with two hydrogens towards the surface). If we expand this PES in a Taylor-series of internal vibrations, we see that the linear terms contain only those vibrations that transform as  $a_1$  in  $C_{3v}$ , respectively,  $C_{2v}$ . These are therefore easier to excite than others; We did not find any appreciable excitation of  $e$  modes of  $C_{3v}$  and the  $a_2$ ,  $b_1$ , and  $b_2$  modes of  $C_{2v}$ .

We will not present results of the simulations with the harmonic PES, because they give almost the same excitation probabilities as the PES with  $V_{\text{Morse}}$ . The maximum excitation probabilities at the surface for the PES with  $V_{\text{Morse}}$  are given in Table V. We have observed the highest excitations for this PES in the  $\nu_4$  umbrella and  $\nu_2$  bending modes in the orientation with two hydrogens, and for the  $\nu_4$  umbrella mode in the orientation with three hydrogens pointing towards the surface. The excitation probabilities for the  $\nu_1$  and  $\nu_3$  stretch modes at this orientations are a factor of magnitude lower.

We have observed higher excitation probabilities for the  $\nu_1$  and  $\nu_3$  stretch modes in the one hydrogen orientation. The excitation probability of the  $\nu_4$  umbrella mode is here lower then for the other orientations, but still in the same order as the stretch modes for this orientation. This can be explained by the values of the  $\alpha$ 's of  $V_{\text{surf}}$  (see Table II) and the force constants of  $V_{\text{harm}}$  (see Table I), because  $V_{\text{harm}}$  is approximately  $V_{\text{Morse}}$  for the ground state. The force constants of  $V_{\text{intra}}$  for the  $\nu_1$  symmetrical stretch stretch and  $\nu_3$  asymmetrical stretch are of the same order, but the  $\alpha$  parameter in  $V_{\text{surf}}$  in the orientation with one hydrogen pointing towards the surface for the  $\nu_3$  asymmetrical stretch is around twice as large as for the  $\nu_1$  symmetrical stretch, which explains why  $\nu_3$  is more excited as  $\nu_1$ . The surface repulsion on the  $\nu_4$  umbrella mode is even three times lower then on the  $\nu_1$  symmetrical stretch mode, but the force constant is also much lower. It results in a little more excitation of the  $\nu_4$  umbrella then in the  $\nu_1$  symmetrical stretch.

For the orientation with two hydrogens pointing towards the surface the repulsion on the vibrational modes is for all modes in the same order ( $\nu_2$  bending a little higher), so the difference in excitation probabilities correlate here primarily with the force constants. The force constants of the  $\nu_2$  bending and  $\nu_4$  umbrella modes are of the same order, as are those of  $\nu_1$  and  $\nu_3$ . The stretch force constants are higher, however, so that the excitation probabilities are lower. The repulsion on the  $\nu_4$  umbrella mode is the largest in the orientation with three hydrogens pointing

towards the surface. The force constants is lower for this modes then for the  $\nu_1$  and  $\nu_3$  stretch modes, so the primary excitation is seen in the  $\nu_4$  umbrella mode.

For the orientation with three hydrogens pointing towards the surface the repulsion on the  $\nu_4$  umbrella mode is the highest in combination with a low force constant, so this mode has a much higher excitation probability than the  $\nu_1$  and  $\nu_3$  stretch modes. Another interesting detail is that the  $\alpha_3$  parameter is higher for the orientation with two than with three hydrogens pointing toward the surface, but the excitation probabilities for the  $\nu_4$  umbrella in this orientations are equal. This is caused by a coupling between the excitation of the  $\nu_2$  bending and the  $\nu_4$  umbrella mode in the orientation with two hydrogens pointing towards the surface.

We observed with  $V_{\text{weak}}$  (see Table V) that all excitation probabilities become much higher than with  $V_{\text{Morse}}$ , except for the  $\nu_4$  umbrella mode with two hydrogens towards the surface, which stays almost the same. It is caused by the fact that, although the  $\nu_1$  symmetrical stretch and  $\nu_3$  asymmetrical stretch contribute almost completely to  $V_{\text{Morse}}$ , the  $\nu_4$  umbrella does so just for a small part. The  $\nu_4$  umbrella contributes primarily, and the  $\nu_2$  bending completely, to the harmonic terms of intramolecular PES  $V_{\text{intra}}$ .  $V_{\text{weak}}$  gives only a lowering in the  $V_{\text{Morse}}$  terms of  $V_{\text{intra}}$ , so we should expect primarily an higher excitation probability in the  $\nu_1$  and  $\nu_3$  stretch modes. This will also cause a higher excitation probability of the other modes, because the turn-around point will be some what later, which give effectively more repulsion on the other modes.

We also observed that for both stretches the excitation probabilities shows the following trend; three hydrogens < two hydrogens < one hydrogen pointing towards the surface. For one hydrogen pointing towards the surface the excitation probability of the  $\nu_3$  asymmetrical stretch is around twice that of the  $\nu_1$  symmetrical stretch, they are almost equal for two hydrogens, and for three hydrogens the  $\nu_1$  is twice the  $\nu_3$  stretch. Some of these trends can also be found for the PES with  $V_{\text{Morse}}$ , but are not always that obvious. They follow the same trends as the  $\alpha$  parameters of  $V_{\text{surf}}$  in Table II.

$V_{\text{shift}}$  (see Table V) gives also higher excitation probabilities for almost all modes than  $V_{\text{Morse}}$ , but for the  $\nu_2$  bending mode in the two hydrogens pointing towards the surface orientation it became lower. This means that the repulsion of the surface is here caused for a large part by the  $V_{\text{shift}}$  terms (see Eq. (22)), where the  $\nu_2$  bending modes don't contribute. It is also in agreement with the fact that we have observed the excitation maximum earlier, so the  $V_{\text{surf}}$  repulsion on the  $\nu_2$  bending modes will be lower. Fig. 1 shows that the repulsion for the PES with  $V_{\text{shift}}$  is stronger than for the other three PESs.

The excitations in the  $\nu_1$  and  $\nu_3$  stretch modes are extremely high with  $V_{\text{shift}}$ , because they contribute strongly to the C-H bond elongation. The trend in the excitation probabilities of the  $\nu_1$  symmetrical stretch mode is caused by the number of bonds pointing towards the surface, because the  $\gamma_{i2}$  parameters are for all bonds and orientations the same, so only the strength of the coupling with the shift-factor dominates. This effect is illustrated in Fig. 2. We didn't observe this trend in the  $\nu_3$  asymmetrical stretch mode, because there is also difference between the  $\gamma_{i4}$  parameters as can be seen in Table III and IV.

## B. Structure Deformation

If we put the methane molecule far from the surface, then all PESs are identical. For this situation we calculated a bond distance of 1.165 Å and bond angle of 109.5 degrees in the ground state. The results of the maximum structure deformations are shown in the Table VI. Fig. 3 shows the names of the bonds and angles for the three orientations.

We observed that the PESs with  $V_{\text{Morse}}$  and  $V_{\text{weak}}$  give again the same trends, but that for the PES with  $V_{\text{weak}}$  these trends are much stronger. This is in agreement with the observations discussed for the excitation probabilities above. The deformations for the PES with  $V_{\text{shift}}$  are dominated by the change of the bond distances for the bonds which are pointing towards the surface. These bonds become longer for all orientations in the same order. So there is no orientational effect and this will be probably caused completely by the  $V_{\text{shift}}$  terms (see Eq. (22)).

For the orientation with one hydrogen pointing towards the surface (see Table VI), we observed that the bond pointing towards the surface becomes shorter, as expected, for the PES with  $V_{\text{Morse}}$  and even more with  $V_{\text{weak}}$ . This is caused by the repulsion of the  $V_{\text{surf}}$  terms, which works in the direction of the bond axes. We observed also some small bond angle deformation. This is probably a secondary effect of the change in the bond distance and correlates to excitation of the  $\nu_4$  umbrella mode. Remarkably, for  $V_{\text{shift}}$  the bond length increases. Clearly the effect of the change in equilibrium bond length is more effective than the repulsion with the surface. The shift effect may be somewhat too large, but the observed change (0.232 Å) is much lower than the shift of the equilibrium (0.54 Å) on which we fitted  $V_{\text{shift}}$ .

We also observed for all orientations with  $V_{\text{shift}}$  an earlier turn-around point, which is in agreement with the earlier observed excitation maximum. This is caused by the extra repulsion contribution in the  $V_{\text{shift}}$  terms and by the longer

bond length; a longer bond gives a higher repulsion for the same position of the center of mass. Fig. 1 shows this effect in the  $\nu_3$  asymmetrical stretch mode.

The orientation with two hydrogens pointing towards the surface (see Table VI) gives also shorter bond distances for the bonds pointing towards the surface for the PESs with  $V_{\text{Morse}}$  and  $V_{\text{weak}}$ , although very little in comparison to the one hydrogen orientation. We expected this, because just half of the repulsion is now in the direction of the bonds. The other half is perpendicular on the C–H bonds and this makes the bond angle larger. The bond angles between the bonds pointing towards the surface show a quite large deformation. This was already expected from the excitation of the  $\nu_2$  bending and  $\nu_4$  umbrella modes.

We also observed that a smaller bond length of the bonds pointing towards the surface correlates with a larger bond angle of the angles between the bonds pointing towards the surface and a higher excitation probability of the  $\nu_2$  bending mode. This can be explained as follows. When the bonds become shorter the center of mass can come closer to the surface. Because of this there will be more repulsion on the  $\nu_2$  bending mode, which will cause a larger bond angle deformation.

Most of the deformations of the other bond angles can be explained as an indirect effect of the deformation of this bond angle, but the deformation of the angle between the bonds pointing away from the surface which was seen at the PES with  $V_{\text{shift}}$  must be caused by the excitation of the  $\nu_4$  umbrella mode.

We observed almost no change in bond length for the PESs with  $V_{\text{Morse}}$  and  $V_{\text{weak}}$  at the three hydrogens towards the surface orientation (see Table VI). Almost all energy is absorbed by the  $\nu_4$  umbrella mode, so this gives quite large bond angle deformations. The bond angle deformation is larger for the PES with  $V_{\text{weak}}$  than with  $V_{\text{Morse}}$  PES; in agreement with higher excitation probability for the PES with  $V_{\text{weak}}$ . The PES with  $V_{\text{shift}}$  has around the same excitation probabilities for the  $\nu_4$  umbrella mode as the PES with  $V_{\text{weak}}$ , but the bond angle deformation is the same as for the PES with  $V_{\text{Morse}}$ . This may be caused by the higher excitations of the  $\nu_1$  and  $\nu_3$  stretch modes and the longer bonds pointing towards the surface at the PES with  $V_{\text{shift}}$ , which can make it harder to deform the bond angles.

### C. Dissociation models

Several dissociation mechanisms for direct methane dissociation on transition metals have been suggested. All proposals can be related to two main ideas. One of them is the breaking of a single C–H bond in the initial collision.<sup>5,31</sup> This model is most suggested in literature and also all wavepacket simulations have focussed on the effects of this model.<sup>25,31–34</sup> The other mechanism is often called “splats” and suggests that the critical requirement for methane dissociation is angular deformation of methane which allows a Ni–C bond to form.<sup>5</sup> Even though we did not try to describe the dissociation itself, we would like to discuss the implication of our simulation for the dissociation.

The “splats” model seems easiest to discuss. Angular deformation is related to the  $\nu_2$  bending and the  $\nu_4$  umbrella mode. The excitation probabilities in Table V seem to indicate that these modes are easy to excite, and that angular deformation should be large. These excitation probabilities are misleading, however. Table VI shows that, although the excitation probabilities depend on the PES, the changes in the bond angles do not. Moreover, these changes are quite small. They are largest for the orientation with two hydrogen atoms pointing towards to surface, for which they are about 8 degrees at most. This seems much too small to enable the formation of a Ni–C bond. A previous estimate of the bond angle deformation gave an energy of 68.1 kJ/mol to get three hydrogens and the carbon in one plane. This correspond to a bond angle of 120 degrees.<sup>5</sup> We find with three hydrogens pointing towards the surface that the bond angle only changes to about 112 degrees at the higher energy of 96 kJ/mol. The reason for this difference is that for the older estimate it was assumed that all translational energy can be used to deform the bond angle, whereas Tables V and VI clearly show that this is not correct.

The excitation probabilities for the stretch modes depend strongly on the orientation of the molecule and on the PES. For the PESs without a change of the equilibrium bond length the excitation probabilities are only appreciably with one hydrogen pointing towards the surface. This is, however, not a favourable orientation for the dissociation. Moreover, Table VI shows that in those cases the repulsion with the surface shortens the C–H bond. The same holds for the orientation with two hydrogens pointing towards the surface, although to a lesser extent, whereas the bond length changes hardly at all with three hydrogens pointing towards the surface. This indicates that the intramolecular PES needs the bond elongation to overcome the repulsion of the surface that shortens the C–H bond, and to get dissociation. This agrees completely with electronic structure calculations that yield a late barrier for dissociation with a very elongated C–H bond.<sup>26,35</sup> The large excitation probabilities for the PES with the elongated equilibrium bond length should not be over-interpreted, however. They are to be expected even if the molecule stays in its (shifted) vibrational ground state. More telling is that for this PES we do find at least some inelastic scattering.

## IV. CONCLUSIONS

We have done wavepacket simulations on the scattering of methane from a flat Ni(111) model surface with a fixed orientation with one, two, or three hydrogens pointing towards the surface. We used the MCTDH method and four different model PESs for each orientation. We used a translational energy of up to 96 kJ/mol and all internal vibrations in the ground state. The scattering was in all cases predominantly elastic.

When the molecule hits the surface, we always observe vibrational excitations of the  $\nu_4$  umbrella and  $\nu_2$  bending modes, especially in the orientations with two or three hydrogens pointing towards the surface. This is due to a favorable coupling that originates from the repulsive interaction with the surface, and the low excitation energies. Deformations of the molecule are predominantly in the bond angles. The changes in the bond angles are, however, too small to allow for the formation of a Ni–C bond, as suggested in the “splats” model of methane dissociation.

Appreciable excitations of the  $\nu_1$  and  $\nu_3$  stretch modes when methane hits the surface are only observed when one hydrogen atom points towards the surface, or when the intramolecular PES has an elongated equilibrium C–H bond length close to the surface. The repulsion of the surface shortens the C–H bond. This can only be overcome when the intramolecular PES incorporates the effect of a longer equilibrium C–H bond length caused by overlap of occupied surface orbitals with the antibonding orbitals of methane. This agrees with quantum chemical calculations, which show a late barrier for dissociation.

The simulations with these model PESs show that the internal vibrations play an important role in the dissociation mechanism. Excitation probabilities when the molecule hits the surface show how the translational energy is converted into vibrational energy and it is distributed over the internal modes. These probabilities vary strongly with the PES. As only few internal vibrations contribute to the dissociation, it is important to obtain more information on the real PES for this system.

## ACKNOWLEDGEMENTS

We would like to thank SON (Stichting Scheikundig Onderzoek in Nederland) and NWO (Nederlandse Organisatie voor Wetenschappelijk Onderzoek) for their financial support.

This work has been performed under the auspices of NIOK, the Netherlands Institute for Catalysis Research, Lab Report No. TUE-98-5-02.

*Copyright 1998 American Institute of Physics. This article may be downloaded for personal use only. Any other use requires prior permission of the author and the American Institute of Physics. This article appeared in J. Chem. Phys. [109, 1966 (1998)] and may be found at <http://link.aip.org/link/?jcp/109/1966> .*

- 
- <sup>1</sup> J.P. Van Hook, Catal. Rev. Sci. Eng. **21**, 1 (1980).
  - <sup>2</sup> C.T. Rettner, H.E. Pfnür, and D.J. Auerbach, Phys. Rev. Lett. **54**, 2716 (1985).
  - <sup>3</sup> C.T. Rettner, H.E. Pfnür, and D.J. Auerbach, J. Chem. Phys. **84**, 4163 (1986).
  - <sup>4</sup> M.B. Lee, Q.Y. Yang, S.L. Tang, and S.T. Ceyer, J. Chem. Phys. **85**, 1693 (1986).
  - <sup>5</sup> M.B. Lee, Q.Y. Yang, and S.T. Ceyer, J. Chem. Phys. **87**, 2724 (1987).
  - <sup>6</sup> S.T. Ceyer, J.D. Beckerle, M.B. Lee, S.L. Tang, Q.Y. Yang, and M.A. Hines, J. Vac. Sci. Technol. A **5**, 501 (1987).
  - <sup>7</sup> J.D. Beckerle, A.D. Johnson, Q.Y. Yang, and S.T. Ceyer, J. Chem. Phys. **91**, 5756 (1989).
  - <sup>8</sup> P.B. Holmbad, J. Wambach, and I. Chorkendorff, J. Chem. Phys. **102**, 8255 (1995).
  - <sup>9</sup> P.B. Holmbad, J. Hvolbæk Larsen, and I. Chorkendorff, J. Chem. Phys. **104**, 7289 (1996).
  - <sup>10</sup> A.C. Luntz and D.S. Bethune, J. Chem. Phys. **90**, 1274 (1989).
  - <sup>11</sup> G.R. Schoofs, C.R. Arumanayagam, M.C. McMaster, and R.J. Madix, Surf. Sci. **215**, 1 (1989).
  - <sup>12</sup> A.V. Hamza and R.J. Madix, Surf. Sci. **179**, 25 (1987).
  - <sup>13</sup> M. Valden, N. Xiang, J. Pere, and M. Pessa, App. Surf. Sci. **99**, 83 (1996).
  - <sup>14</sup> M. Valden, J. Pere, N. Xiang, and M. Pessa, Chem. Phys. Lett. **257**, 289 (1996).
  - <sup>15</sup> R.W. Verhoef, D. Kelly, C.B. Mullins, and W.H. Weinberg, Surf. Sci. **287**, 94 (1993).
  - <sup>16</sup> R.W. Verhoef, D. Kelly, C.B. Mullins, and W.H. Weinberg, Surf. Sci. **311**, 196 (1994).
  - <sup>17</sup> R.W. Verhoef, D. Kelly, C.B. Mullins, and W.H. Weinberg, Surf. Sci. **325**, 93 (1995).
  - <sup>18</sup> D.C. Seets, M.C. Wheeler, and C.B. Mullins, J. Chem. Phys. **107**, 3986 (1997).
  - <sup>19</sup> T.P. Beebe, Jr., D.W. Goodman, B.D. Kay, and J.T. Yates, Jr., J. Chem. Phys. **87**, 2305 (1987).

- <sup>20</sup> I. Chorkendorff, I. Alstrup, and S. Ullmann, *Surf. Sci.* **227**, 291 (1990).
- <sup>21</sup> L. Hanley, Z. Xu, J.T. Yates, Jr., *Surf. Sci. Lett.* **248**, L265 (1991).
- <sup>22</sup> R.A. Campbell, J. Szanyi, P. Lenz, and D.W. Goodman, *Catal. Lett.* **17**, 39 (1993).
- <sup>23</sup> A.C. Luntz, and H.F. Winters, *J. Chem. Phys.* **101**, 10980 (1994).
- <sup>24</sup> B. Ølgaard Nielsen, A.C. Luntz, P.M. Holmblad, I. Chorkendorff, *Catal. Lett.* **32**, 15 (1995).
- <sup>25</sup> A.P.J. Jansen and H. Burghgraef, *Surf. Sci.* **344**, 149 (1995).
- <sup>26</sup> H. Burghgraef, A.P.J. Jansen, and R.A. van Santen, *J. Chem. Phys.* **98**, 8810 (1993).
- <sup>27</sup> H. Burghgraef, A.P.J. Jansen, and R.A. van Santen, *Chem. Phys.* **177**, 407 (1993).
- <sup>28</sup> H. Burghgraef, A.P.J. Jansen, and R.A. van Santen, *Faraday Discuss. Chem. Soc.* **96**, 337 (1993).
- <sup>29</sup> H. Burghgraef, A.P.J. Jansen, and R.A. van Santen, *J. Chem. Phys.* **101**, 11012 (1994).
- <sup>30</sup> H. Burghgraef, A.P.J. Jansen, and R.A. van Santen, *Surf. Sci.* **324**, 345 (1995).
- <sup>31</sup> A.C. Luntz, and J. Harris, *Surf. Sci.* **258**, 397 (1991).
- <sup>32</sup> A.C. Luntz, and J. Harris, *J. Vac. Sci. A* **10**, 2292 (1992).
- <sup>33</sup> A.C. Luntz, *J. Chem. Phys.* **102**, 8264 (1995).
- <sup>34</sup> M.-N. Carré, and B. Jackson, *J. Chem. Phys.* **108**, 3722 (1998).
- <sup>35</sup> P. Kratzer, B. Hammer, and J.K. Nørskov, *J. Chem. Phys.* **105**, 5595 (1996).
- <sup>36</sup> H. Yang, and J.L. Whitten, *J. Chem. Phys.* **96**, 5529 (1992).
- <sup>37</sup> M.-S. Liao, C.-T. Au, and C.-F. Ng, *Chem. Phys. Lett.* **272**, 445 (1997).
- <sup>38</sup> V.A. Ukraintsev, and I. Harrison, *J. Chem. Phys.* **101**, 1564 (1994).
- <sup>39</sup> J.A. Stinnett, and R.J. Madix, *J. Chem. Phys.* **105**, 1609 (1996).
- <sup>40</sup> U. Manthe, H.-D. Meyer, and L.S. Cederbaum, *J. Chem. Phys.* **97**, 3199 (1992).
- <sup>41</sup> A.P.J. Jansen, *J. Chem. Phys.* **99**, 4055 (1993).
- <sup>42</sup> U. Manthe, H.-D. Meyer, and L.S. Cederbaum, *J. Chem. Phys.* **97** (1992) 9062.
- <sup>43</sup> U. Manthe, and A.D. Hammerich, *Chem. Phys. Lett.* **211** 7 (1993).
- <sup>44</sup> A.D. Hammerich, U. Manthe, R. Kosloff, H.-D. Meyer, and L.S. Cederbaum, *J. Chem. Phys.* **101** 5623 (1994).
- <sup>45</sup> L. Liu, J.-Y. Fang, and H. Guo, *J. Chem. Phys.* **102** 2404 (1995).
- <sup>46</sup> J.-Y. Fang and H. Guo, *J. Chem. Phys.* **102** 1944 (1995).
- <sup>47</sup> J.-Y. Fang and H. Guo, *J. Chem. Phys.* **101** 5831 (1994).
- <sup>48</sup> J.-Y. Fang and H. Guo, *Chem. Phys. Lett.* **235** 341 (1995).
- <sup>49</sup> A. Capellini, A.P.J. Jansen, *J. Chem. Phys.* **104**, 3366 (1996).
- <sup>50</sup> G.A. Worth, H.-D. Meyer, and L.S. Cederbaum, *J. Chem. Phys.* **105**, 4412 (1996).
- <sup>51</sup> A. Jäckle, and H.-D. Meyer, *J. Chem. Phys.* **105**, 6778 (1996).
- <sup>52</sup> T. Gerdts, and U. Manthe, *J. Chem. Phys.* **107**, 6584 (1997).
- <sup>53</sup> M.H. Beck, and H.-D. Meyer, *Z. Phys. D* **42**, 113 (1997).
- <sup>54</sup> *The NAG Fortran Library Manual, Mark 16*, Vol. 2 (NAG Ltd., Oxford, 1993) routine D02CBF.
- <sup>55</sup> E.B. Wilson, J.C. Decius, and P.C. Cross, *Molecular Vibrations. The Theory of Infrared and Raman Spectra*. (McGraw-Hill, London, 1955).
- <sup>56</sup> D.L. Gray and A.G. Robiette, *Mol. Phys.* **37**, 1901 (1979).
- <sup>57</sup> T.J. Lee, J.M.L. Martin, and P.R. Taylor, *J. Chem. Phys.* **102**, 254 (1995).
- <sup>58</sup> J.C. Light, I.P. Hamilton, and J.V. Lill, *J. Chem. Phys.* **82**, 1400 (1985).
- <sup>59</sup> R.D. Levine, and R.B. Bernstein, *Molecular Reaction Dynamics and Chemical Reactivity*. (Oxford University Press, Oxford, 1987).

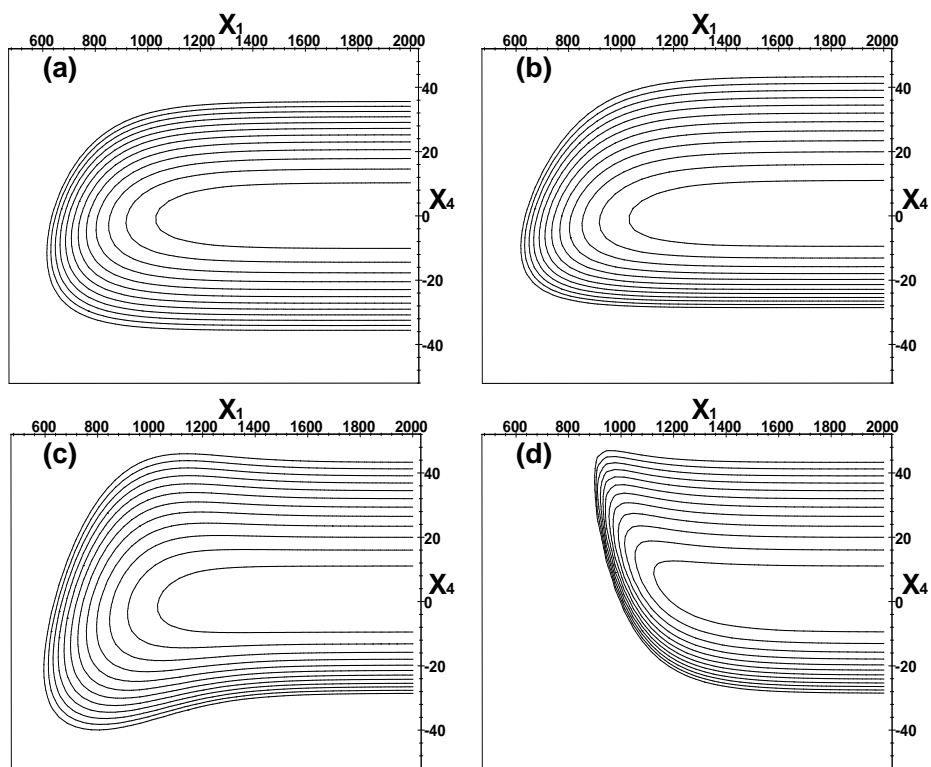


FIG. 1. Contour plots in the energy range from 0 to 0.12 Hartree of a cross-section in the orientation with one hydrogen atom pointing towards the surface for the translational mode  $X_1$  and the  $\nu_3$  asymmetrical mode  $X_4$  (an  $a_1$  mode in  $C_{3v}$ ), both in atomic displacement, which show well the different behaviours of the four PESs; (a) harmonic PES, (b) an anharmonic intramolecular PES, (c) intramolecular PES with weakening C–H bond, and (d) intramolecular PES with elongation of the C–H bond. All other coordinates set to zero.

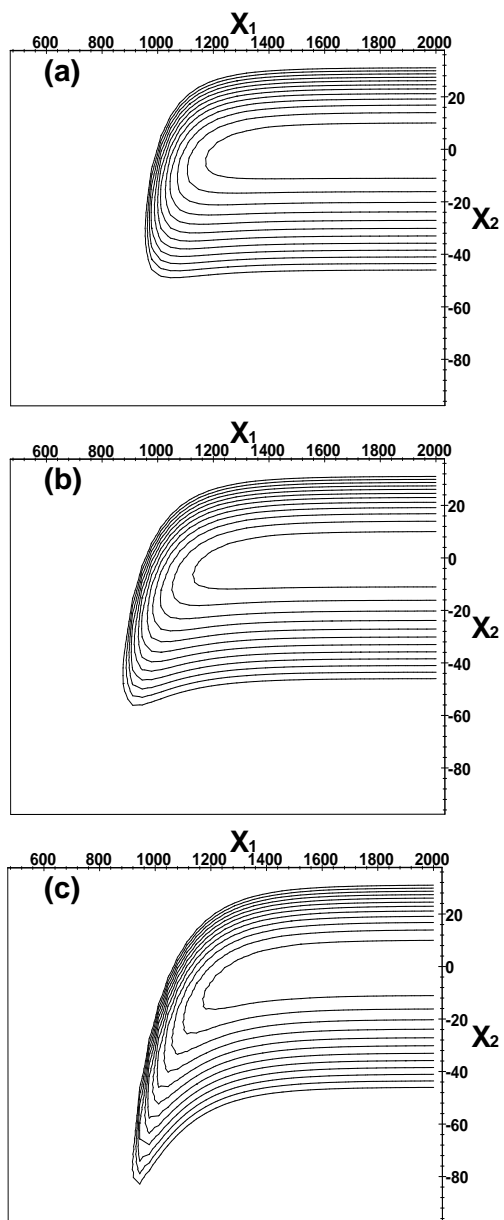


FIG. 2. Contour plots in the energy range from 0 to 0.12 Hartree of a cross-section of the PES with elongation of the C–H bond in the translational  $X_1$  and the  $\nu_1$  symmetrical stretch mode  $X_2$ , both in atomic displacement; (a) one, (b) two, and (c) three hydrogens pointing towards the surface. All other coordinates set to zero.

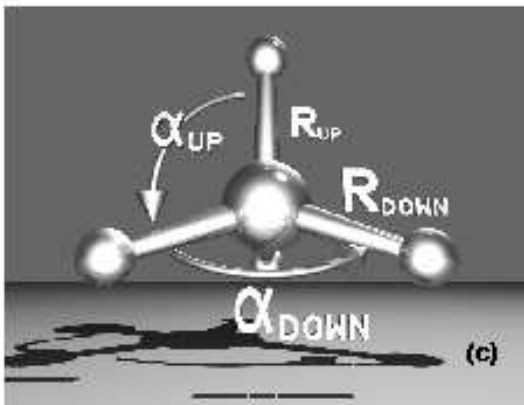
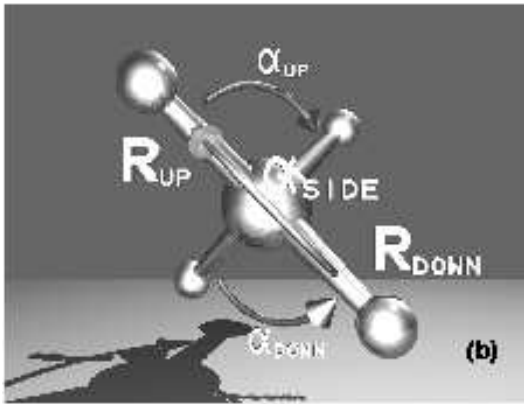
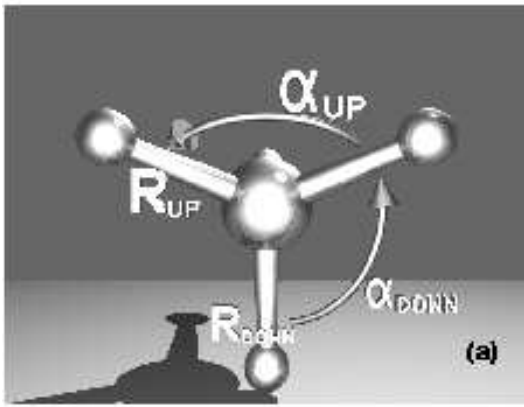


FIG. 3. Schematic representation of the  $R_{\text{down}}$  and  $R_{\text{up}}$  bonds, and the  $\alpha_{\text{down}}$ ,  $\alpha_{\text{side}}$  and  $\alpha_{\text{up}}$  angles for the three orientations: (a) one, (b) two, and (c) three hydrogens pointing towards the surface.

TABLE I. Overview of the relations between the mass-weighted coordinates  $X_i$ ; the force constants  $k_i$  (in atomic units), the designation, and the symmetry in  $T_d$ ,  $C_{3v}$  and  $C_{2v}$ .

$i$	$k_i$	designation	$T_d$	$C_{3v}$	$C_{2v}$
1		translation	$t_2$	$a_1$	$a_1$
2	$1.780 \cdot 10^{-4}$	$\nu_1$ ; symmetrical stretch	$a_1$	$a_1$	$a_1$
3	$3.599 \cdot 10^{-5}$	$\nu_4$ ; umbrella	$t_2$	$a_1$	$a_1$
4	$1.892 \cdot 10^{-4}$	$\nu_3$ ; asymmetrical stretch	$t_2$	$a_1$	$a_1$
5	$4.894 \cdot 10^{-5}$	$\nu_2$ ; bending	$e$	$e$	$a_1$
6	$4.894 \cdot 10^{-5}$	$\nu_2$ ; bending	$e$	$e$	$a_2$
7	$3.599 \cdot 10^{-5}$	$\nu_4$ ; umbrella	$t_2$	$e$	$b_1$
8	$3.599 \cdot 10^{-5}$	$\nu_4$ ; umbrella	$t_2$	$e$	$b_2$
9	$1.892 \cdot 10^{-4}$	$\nu_3$ ; asymmetrical stretch	$t_2$	$e$	$b_1$
10	$1.892 \cdot 10^{-4}$	$\nu_3$ ; asymmetrical stretch	$t_2$	$e$	$b_2$

TABLE II.  $\alpha$  and  $\beta$  values (in atomic units) of  $V_{\text{surf}}$  with one, two or three hydrogens pointing towards the surface (see Eqs. (14), (15) and (16)).

	one	two	three
$\alpha_1$	$6.281 \cdot 10^{-3}$	$6.281 \cdot 10^{-3}$	$6.281 \cdot 10^{-3}$
$\alpha_2$	$1.256 \cdot 10^{-2}$	$7.252 \cdot 10^{-3}$	$4.187 \cdot 10^{-3}$
$\alpha_3$	$4.226 \cdot 10^{-3}$	$-7.931 \cdot 10^{-3}$	$-1.198 \cdot 10^{-2}$
$\alpha_4$	$-2.040 \cdot 10^{-2}$	$-7.445 \cdot 10^{-3}$	$-3.128 \cdot 10^{-3}$
$\alpha_5$		$-1.026 \cdot 10^{-2}$	
$\beta_1$			$5.921 \cdot 10^{-3}$
$\beta_2$			$1.026 \cdot 10^{-2}$
$\beta_3$		$6.079 \cdot 10^{-3}$	$2.866 \cdot 10^{-3}$
$\beta_4$			$4.963 \cdot 10^{-3}$
$\beta_5$		$6.476 \cdot 10^{-3}$	$3.053 \cdot 10^{-3}$
$\beta_6$			$5.288 \cdot 10^{-3}$

TABLE III.  $\gamma$  values (in atomic units) of  $V_{\text{Morse}}$  with one and three hydrogens pointing towards the surface (see Eq. (18)).

one	three	value
$\gamma_{12}, \gamma_{22}, \gamma_{32}, \gamma_{42}$	$\gamma_{12}, \gamma_{22}, \gamma_{32}, \gamma_{42}$	$1.079 \cdot 10^{-2}$
$\gamma_{13}, -3\gamma_{23}, -3\gamma_{33}, -3\gamma_{43}$	$-\gamma_{13}, 3\gamma_{23}, 3\gamma_{33}, 3\gamma_{43}$	$1.359 \cdot 10^{-3}$
$\gamma_{14}, -3\gamma_{24}, -3\gamma_{34}, -3\gamma_{44}$	$-\gamma_{14}, 3\gamma_{24}, 3\gamma_{34}, 3\gamma_{44}$	$-1.966 \cdot 10^{-2}$
$\gamma_{17}, \gamma_{18}, \gamma_{19}, \gamma_{1,10}, \gamma_{28}, \gamma_{2,10}$	$\gamma_{17}, \gamma_{18}, \gamma_{19}, \gamma_{1,10}, \gamma_{28}, \gamma_{2,10}$	0.0
$\gamma_{27}, -2\gamma_{37}, -2\gamma_{47}$	$-\gamma_{27}, 2\gamma_{37}, 2\gamma_{47}$	$1.282 \cdot 10^{-3}$
$\gamma_{38}, -\gamma_{48}$	$\gamma_{38}, -\gamma_{48}$	$-1.110 \cdot 10^{-3}$
$\gamma_{29}, -2\gamma_{39}, -2\gamma_{49}$	$-\gamma_{29}, 2\gamma_{39}, 2\gamma_{49}$	$-1.853 \cdot 10^{-2}$
$\gamma_{3,10}, -\gamma_{4,10}$	$-\gamma_{3,10}, \gamma_{4,10}$	$1.605 \cdot 10^{-2}$

TABLE IV.  $\gamma$  values (in atomic units) of  $V_{\text{Morse}}$  with two hydrogens pointing towards the surface (see Eq. (18)).

two	value
$\gamma_{12}, \gamma_{22}, \gamma_{32}, \gamma_{42}$	$1.079 \cdot 10^{-2}$
$\gamma_{13}, \gamma_{23}, -\gamma_{33}, -\gamma_{43}, \gamma_{17}, -\gamma_{27}, \gamma_{37}, -\gamma_{47}, \gamma_{18}, -\gamma_{28}, -\gamma_{38}, \gamma_{48}$	$-7.849 \cdot 10^{-4}$
$\gamma_{14}, \gamma_{24}, -\gamma_{34}, -\gamma_{44}, \gamma_{19}, -\gamma_{29}, \gamma_{39}, -\gamma_{49}, \gamma_{1,10}, -\gamma_{2,10}, -\gamma_{3,10}, \gamma_{4,10}$	$1.135 \cdot 10^{-2}$

TABLE V. Excitation probabilities, at an initial translational energy of 96 kJ/mol and all initial vibrational states in the ground state, for the three different PESs in the  $a_1$  modes of the  $C_{3v}$  and  $C_{2v}$  symmetry, with one, two or three hydrogens pointing towards the surface. These modes are a  $\nu_1(a_1)$  symmetrical stretch, a  $\nu_2(e)$  bending, a  $\nu_3(t_2)$  asymmetrical stretch, and a  $\nu_4(t_2)$  umbrella in the  $T_d$  symmetry. The PESs are: An anharmonic intramolecular PES (Morse, see Eq. (18)), an intramolecular PES with weakening C–H bonds (weak, see Eq. (20)), and an intramolecular PES with elongation of the C–H bonds (shift, see Eq. (22)).

orientation	PES	$\nu_1(a_1)$ stretch	$\nu_2(e)$ bending	$\nu_3(t_2)$ stretch	$\nu_4(t_2)$ umbrella
one	Morse	0.023		0.054	0.030
	weak	0.135		0.308	0.075
	shift	0.340		0.727	0.067
two	Morse	0.010	0.108	0.009	0.104
	weak	0.067	0.135	0.073	0.107
	shift	0.707	0.065	0.768	0.331
three	Morse	0.003		0.006	0.102
	weak	0.038		0.019	0.208
	shift	0.819		0.674	0.214

TABLE VI. Structure deformation, at an initial translational energy of 96 kJ/mol and all initial vibrational states in the ground state, with one, two, and three hydrogen pointing towards the surface for three different PESs: An anharmonic intramolecular PES (Morse, see Eq. (18)), an intramolecular PES with weakening C–H bonds (weak, see Eq. (20)), and an intramolecular PES with elongation of the C–H bonds (shift, see Eq. (22)). See Fig.3 for the meaning  $R_{\text{down}}$ ,  $R_{\text{up}}$ ,  $\alpha_{\text{down}}$ ,  $\alpha_{\text{up}}$ , and  $\alpha_{\text{side}}$ . All bond distances are given in Å and all bond angles are given in degrees. The gas phase values correspond to the bond distance and angles far from the surface, and are the same for all three PES types.

Orientation	PES	$R_{\text{down}}$	$R_{\text{up}}$	$\alpha_{\text{down}}$	$\alpha_{\text{up}}$	$\alpha_{\text{side}}$
gas phase	all	1.165		109.5		
one	Morse	1.123	1.166	108.5	110.4	
	weak	1.051	1.167	108.2	110.7	
	shift	1.397	1.158	109.9	109.0	
two	Morse	1.157	1.165	116.7	108.9	107.8
	weak	1.137	1.163	117.6	109.0	107.5
	shift	1.386	1.159	115.7	106.9	108.5
three	Morse	1.164	1.160	111.2	107.7	
	weak	1.167	1.155	112.4	106.3	
	shift	1.389	1.144	111.2	107.7	